IMPACT ON AIR QUALITY BY INCREASE IN AIR POLLUTANT EMISSIONS FROM THERMAL POWER PLANTS

Akira Kondo[1], Hikari Shimadera[1] and Mai Chinzaka[1]

[1]Osaka University, Japan

ABSTRACT: The amount of thermal power generation has increased significantly in Japan since the Great East Japan Earthquake in 2011, resulting in increase in emissions of air pollutants. This research evaluated the impact of the emission increase on air quality in Kinki region, Japan by using the Community Multiscale Air Quality model (CMAQ) driven by the Weather Research and Forecasting model (WRF). Three cases of CMAQ simulations were conducted with emission data considering thermal power generation for the year 2010 and 2012, and without power plant emissions, using the meteorological field fixed to 2010.The simulation for the year 2010 well agreed with observations. The emission increase caused higher air pollutant concentrations around power plants, and the contribution of power plant emissions was up to 15 % of NO2 concentration in 2012.

Keywords: Thermal Power Plant, Air Quality Model, Meteorological Model, Nitrogen Dioxide, Sulfur Dioxide

1. INTRODUCTION

The amount of thermal power generation has significantly increased in Japan since the accident of Fukushima Daiichi nuclear power station due to the Great East Japan Earthquake in 2011. The ratio of nuclear power generation to the total power generation in the major 10 companies in Japan was 29% in 2010. In 2012 after the Great East Japan Earthquake, it decreased in 2%. The ratio of thermal power generation rapidly increased from 62% to 89%. As the power generation in the Kinki district of Japan depended heavily on nuclear power generation, the ratio of thermal power generation increased from 46% to 80%[1]. It resulted in the increase in emissions of air pollutants. It is important to assess air quality by the increased air pollutants in the view of the environmental conservation.

In this study, the simulations of air quality by the increased air pollutants from thermal power generation after the Great East Japan Earthquake were carried out in the Kinki district by using air quality model.

2. CALCULATION CONDITIONS

2.1 Outline of Model

The air quality was simulated by Community Multiscale Air Quality system (CMAQ5.02), which was developed by United States Environmental Protection Agency. The meteorological data was provided from the simulation by Weather Research Forecasting model (WRF3.51), which was developed by National Center for Atmospheric Research. The configuration of WRF and CMAQ used in this study is shown in Table 1.

Table 1 WRF/CMAQ configurations

Parameter	Setting
WRF	
Version	ARW 3.5.1
Initial and boundary	NCEP FNL, MSM-GPV, RTG-SST-HR
Land use	USGS 24-category data
Horizontal grid number	98×88 (D1), 108×120 (D2), 92×92(D3)
Vertical grid number	30 (surface-100 hPa layer)
Explicit moisture	WSM-6
Cumulus	Kain-Fritsch
PBL	YSU scheme
Surface layer	Noah land-surface model
Radiation	RRTM and Dudhia
Parameter	**Setting**
CMAQ	
Version	5.0.2
Horizontal grid number	76×76 (D1), 92×104 (D2), 76×76(D3)
Initial and boundary	Made from MOZART-4
Baseline emission	INTEX-B, JATOP(vehiecle), OPRF(ship), EAGrid2010-JAPAN
Horizontal/vertical advection	WRF-based scheme
Horizontal/vertical diffusion	Multiscale/ACM2
Photolysis calculation	CCTM in-line calculation
Gas phase chemistry	CB05
Aerosol	AERO 6

Three simulations were carried out against varying emissions from power generation; use of the emissions in 2010 (2010case); use of the emissions in 2012 (2012case) and not considering the emissions from power generation (base).

The boundary conditions of CMAQ were set to the calculations by Model for Ozone and Related Chemical Tracers version 4 (MOZART-4).

2.2 Calculation Period and domain

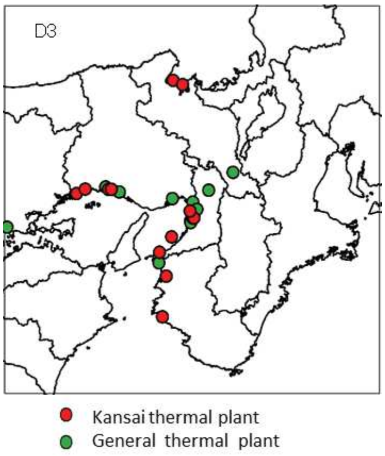

Fig. 1 Location of thermal power plants in D3

Meteorology simulations were conducted by using WRF from April 2010 to March 2011 with an initial spin-up period of 22-31 March 2010. The calculation domains include domain 1 (D1) covering a wide area of Northeast Asia, domain 2 (D2) covering almost the entire area of Japan and domain 3(D3) covering the Kinki district. The horizontal resolutions and the number of grid cells are 64 km and 76 × 76 for D1, 16 km and 92 × 104 for D2, and 4 km and 76 × 76 for D3, respectively. The vertical layers consist of 30 sigma-pressure coordinated layers from the surface to 100 hPa with the middle height of the first layer being approximately 28 m. Figure 1 shows the domain 3 and the location of the thermal power plants.

2.3 Emissions from thermal power stations

The emissions of NOx, SO_2, PM_{10}, $PM_{2.5}$, NH_3 from thermal power stations shown in Figure 1 were estimated. The emissions of NOx, SO_2 from the thermal power stations in the Kansai Electric Power Co. were given from the electric power generation performance in 2014[2]. The emissions of PM_{10}, $PM_{2.5}$, NH_3 were estimated from the emission database of EAGrid2010-JAPAN [3] in 2010 and fuel consumption in 2010 and 2012. The ratio of oil consumption, LNG consumption and coal consumption in 2010 and 2012 is 4.19, 1.56, and 1.15, respectively. The emissions from the thermal power stations in other companies were predicted from the electric power generation ratio in the Kansai Electric Power Co. and other companies. The hourly variation of the emissions each month were considered from the hourly variation of the electric power generation in 2012[4].

Figure 2 shows the emissions of NOx and SO_2 each power stations in 2010 and 2011. In the Kainan oil power station, the emissions extremely increased in 2012, because the Kainan oil power station was the peak load electricity source. On the other hand, the emissions in the Kobe coal power station in 2012 were almost same as 2010, because the Kobe coal power station was used as the base load electricity source.

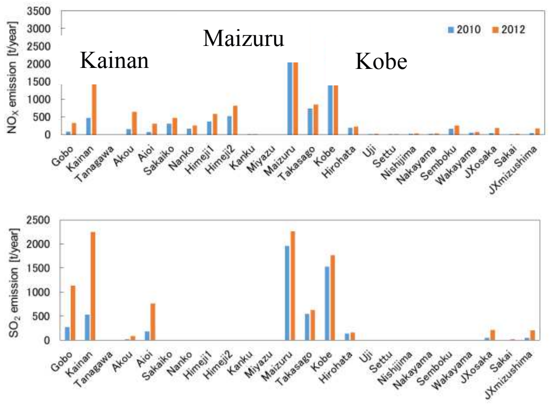

Fig.2 NO_X and SO_2 emissions from thermal plant in 2010 and 2012

3. RESULTS

3.1 Comparison between simulations and observations

The simulations in WRF and CMAQ and the observations were compared by several statistical indexes, which were correlation confident (R), Mean Absolute Error (MAE), Mean Bias Error (MBE) and Index of Agreement (IA). Table 2 shows the statistical indexes of mean daily temperature, specific humidity and wind speed on April, July, October and January in 2010 Japan fiscal year at several monitoring stations in Osaka prefecture simulated by WRF. The criteria of the statistical indexes, which were MBE ≦ ± 0.5°C, MAE≦2°C, IA ≧0.8 for temperature, MBE≦±1 g/ kg, MAE≦2 g/kg, IA≧0.6 for mixing ratio and MBE ≦ ± 0.5 m/s, RMSE ≦ 2 m/s, IA ≧ 0.6 for wind speed, was proposed by Emery[5]. Except for MBE of temperature on January, temperature, mixing ratio and wind speed satisfied the criteria. Figure 3 shows the mean daily variations of temperature, mixing ratio and wind speed in 2010 Japan fiscal year at several monitoring stations in Osaka prefecture. The simulations well captured the observations. Table 3 shows the statistical indexes of mean daily NO_2, SO_2 $PM_{2.5}$ and O_3 in 2010 Japan fiscal year at several monitoring stations in Osaka prefecture simulated by CMAQ. Figure 4 shows the mean daily variations of NO_2, SO_2 $PM_{2.5}$ and O_3 concentration in 2010 Japan fiscal year at several monitoring stations in Osaka prefecture. The simulations well captured the observations.

Table 2 Statistical indexes of temperature, mixing ratio and wind speed in Osaka prefecture

Statistic	Apr.	Jul.	Oct.	Jan.
Temperature (2010JFY)				
number	720	744	744	744
Obs.ave	13.56	27.91	19.91	4.36
Sim.ave	13.15	28.33	20.37	3.29
R	0.96	0.89	0.95	0.90
MBE	--0.42	0.42	0.47	-1.07
MAE	0.94	1.00	0.84	1.25
IA	0.97	0.93	0.97	0.90
Mixing ratio (2010JFY)				
number	720	744	744	744
Obs.ave	5.66	16.42	9.30	2.73
Sim.ave	5.73	16.39	9.65	2.97
R	0.95	0.65	0.93	0.81
MBE	0.08	-0.03	0.36	0.24
MAE	0.53	0.86	0.71	0.35
IA	0.97	0.81	0.96	0.86
Wind Speed (2010JFY)				
number	720	743	744	744
Obs.ave	2.63	2.54	2.11	3.08
Sim.ave	2.76	2.82	2.56	2.72
R	0.69	0.68	0.65	0.70
MBE	0.12	0.28	0.45	-0.35
MAE	1.28	1.26	1.09	1.48
IA	0.82	0.81	0.77	0.82

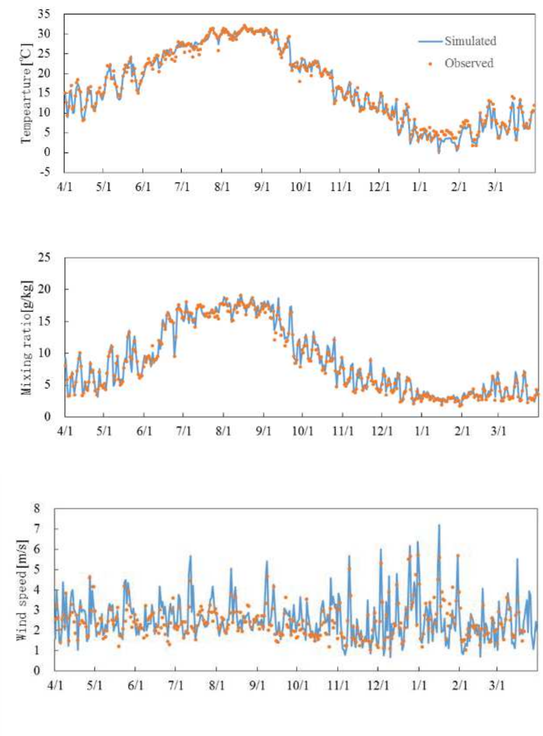

Fig.3 mean daily variations of temperature, mixing ratio and wind speed in 2010 Japan fiscal year

Table 3 Statistical indexes of NO_2, SO_2 $PM_{2.5}$ and O_3 concentration in Osaka prefecture

Statistic	NO_2	SO_2	$PM_{2.5}$	O_3
number	358	363	358	360
Obs.ave	22.03	4.77	19.21	49.82
Sim.ave	21.80	3.05	14.27	49.17
R	0.85	0.65	0.88	0.84
MBE	-0.23	-1.72	-4.95	-0.66
MAE	4.04	2.00	5.70	7.79
IA	0.91	0.69	0.89	0.90

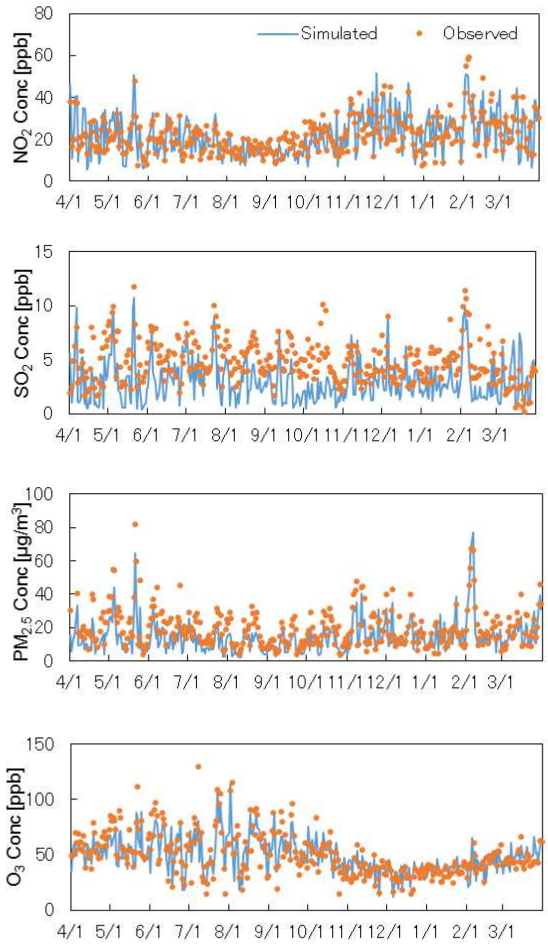

Fig.4 mean daily variations of NO_2, SO_2 $PM_{2.5}$ and O_3 concentration in 2010 Japan fiscal year

3.2 Contribution to Air Quality by emissions from thermal power stations

The detail analysis was performed at the neighborhood of Kainan thermal power station and the Kobe thermal power station in which the pollutant emissions extremely increased in 2012 Figure 5 shows the NO_2 concentration in 2012, the contribution to NO_2 concentration by the emissions from thermal power station in 2010 (2010-base) and the contribution to NO_2 concentration by the increment emissions from thermal power station in 2012 (2012-2010) at the Kainan and Kobe. The mean NO_2 concentration, the mean contribution NO_2 concentration and the mean contribution rate was 6.2ppb, 0.8ppb and 13.4% at the Kainan and 11.6ppm, 0.2ppb and 2.0% at the Kobe, respectively. NO_2 concentration in the maximum contribution by the emission from the thermal power station was 24.1ppb at the Kainan on 6 December and 20.5ppm at the Kobe on 13 March, respectively. The contribution NO_2 concentration and the contribution rate on the above day was 3.7ppb and 15.3% at the Kainan and 1.1ppb and 5.1% at the Kobe, respectively.

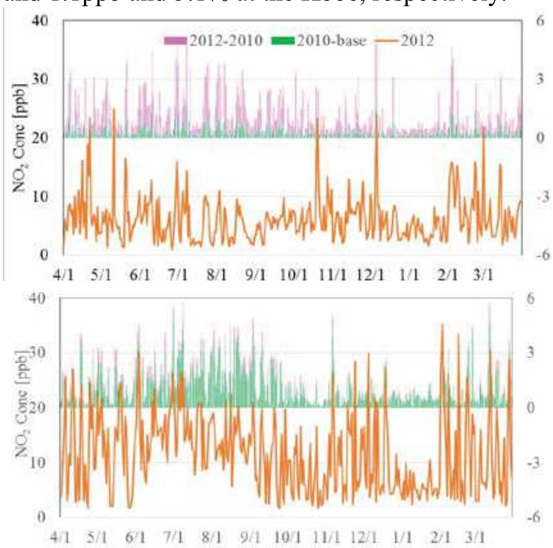

Fig.5 Time series of NO_2 concentration and the contribution to NO_2 from thermal power station at Kainan (top) and Kobe (bottom).

Figure 6 shows the distribution of NO_2 concentration in D3 and D1, and the distribution of the incremental NO_2 concentration at 7 JST of 1 July, when the contribution to NO_2 concentration by the increment emissions from thermal power station at Kainan was maximum by the simulation. The transboundary pollution of NO_2 didn't occurred in the simulation in D3. In the coast areas and the industry areas, the high NO_2 concentration occurred in the simulation in D1, because the main emissions of NO_2 was from factory, vehicles and vessels. The remarkable increase of NO_2 concentration occurred at the Kainan and at the Maizuru faced to Japan Sea. The increase of NO_2 concentration at the Kobe was small compared at the Kainan. The spread of NO_2 concentration from the power stations was limited.

Figure 7 shows the SO_2 concentration in 2012, the contribution to SO_2 concentration by the emissions from thermal power station in 2010 (2010-base) and the contribution to SO_2

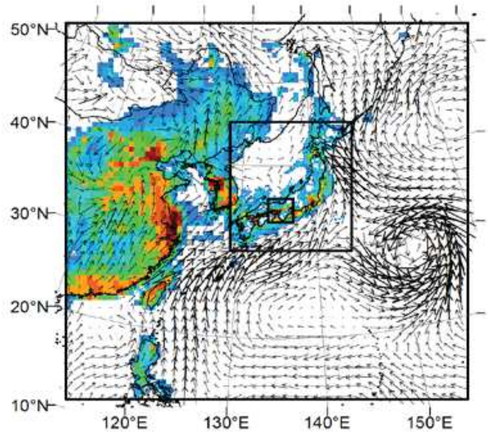

concentration by the increment emissions from thermal power station in 2012 (2012-2010) at the Kainan and Kobe. The mean SO_2 concentration,

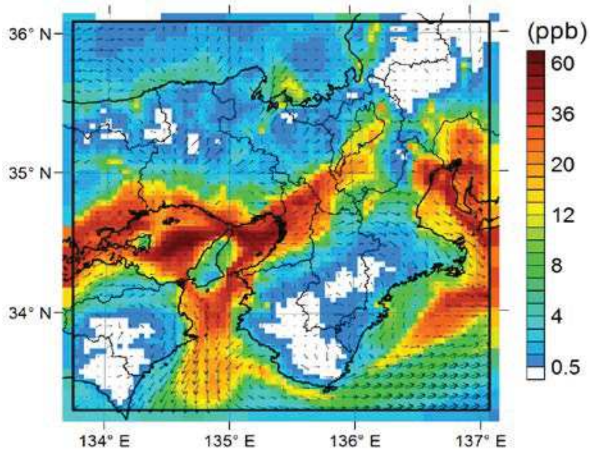

the mean contribution SO_2 concentration and the mean contribution rate was 3.3ppb, 0.9ppb and 26.0% at

Fig.6 Distribution of NO_2 concentration in D3 (Top) and D1 (Middle), and the distribution of the incremental NO_2 concentration (Bottom) at 7 JST of 1 July

the Kainan and 4.0ppm, 0.2ppb and 3.7% at the Kobe, respectively. SO_2 concentration in the maximum contribution by the emission from the thermal power station was 13.3ppb at the Kainan on 6 December and 12.0ppm at the Kobe on 5 May, respectively. The contribution SO_2 concentration and the contribution rate on the above day was 4.2ppb and 32.0% at the Kainan and 0.6ppb and 5.4% at the Kobe, respectively.

Figure 8 shows the distribution of SO_2 concentration in D3 and D1, and the distribution of the incremental SO_2 concentration at 7 JST of 5 May, when the contribution to SO_2 concentration by the increment emissions from thermal power station at Kainan was maximum by the simulation. The transboundary pollution of SO_2 didn't occurred in the simulation in D3. In the coast areas and the industrial areas, the high SO_2 concentration occurred in the simulation in D1, because the main emissions of SO_2 was from factory and vessels. The remarkable increase of SO_2 concentration occurred at the Kainan. The increase of SO_2 concentration at the almost thermal power stations occurred. SO_2 concentration diffused in the wide area.

The contribution rate of NO_2 and SO_2 concentration by the emission from the thermal power station was almost same for the mean concentration and for the maximum concentration. These results suggested that the difference of the contribution concentration occurred from the difference of the meteorological conditions. SO_2 concentration relatively diffused in the wide area compared with NO_2 concentration, because NO_2 was more reactive chemicals in the atmosphere.

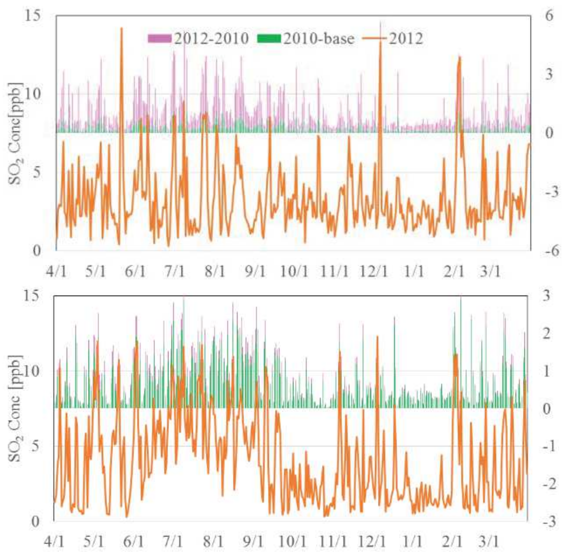

Fig.7 Time series of SO_2 concentration and the contribution to SO_2 from thermal power station at Kainan (top) and Kobe (bottom).

Figure 9 shows the O_3 concentration in 2012, the contribution to O_3 concentration by the emissions from thermal power station in 2010 (2010-base) and the contribution to O_3 concentration by the increment emissions from thermal power station in 2012 (2012-2010) at the Kainan and Kobe. The maximum O_3 concentration and the mean contribution O_3 concentration was 53ppb and -0.9ppb at the Kainan and 99ppm and -0.08ppb at the Kobe, respectively. The contribution O_3 concentration by the emission from the thermal power station became negative because of NO titration.

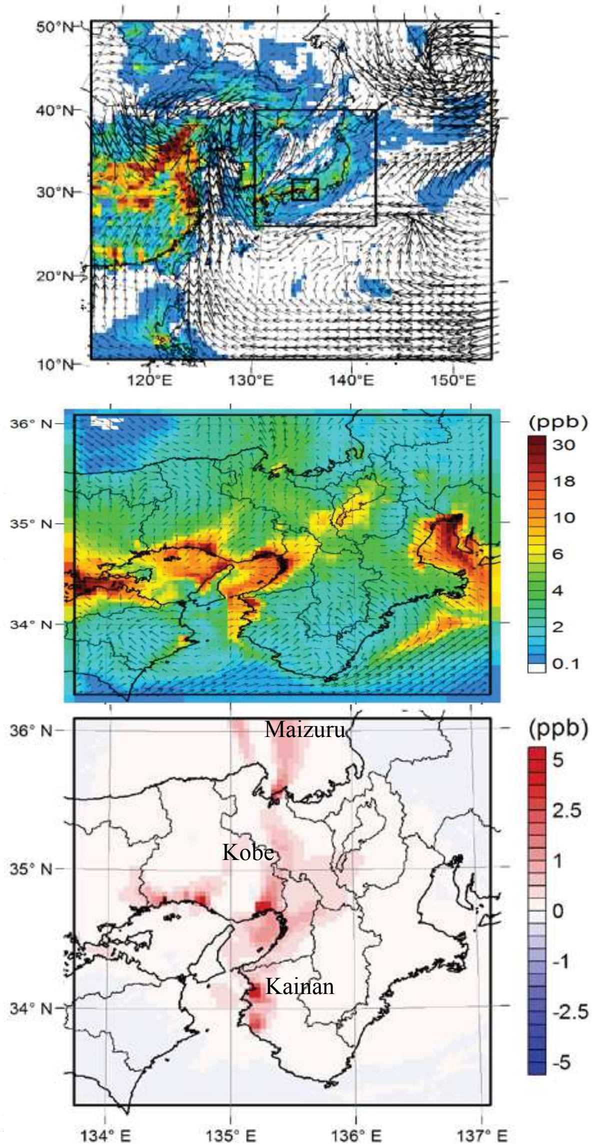

Fig.8 Distribution of SO_2 concentration in D3 (Top) and D1 (Middle), and the distribution of the incremental SO_2 concentration (Bottom) at 7 JST of 5 May

Figure 10 shows the distribution of O_3 concentration in D3 and D1, and the distribution of the incremental O_3 concentration at 18 JST of 2 August, when O_3 concentration became maximum at Kainan by the simulation. O_3 concentration in the simulation in D1 became high in inland that was apart from urban area with much air pollution emissions. Due to the increment of emissions from thermal power stations, O_3 concentration increased in the wide area of D1 except for the neighborhood of the thermal power stations because of NO titration.

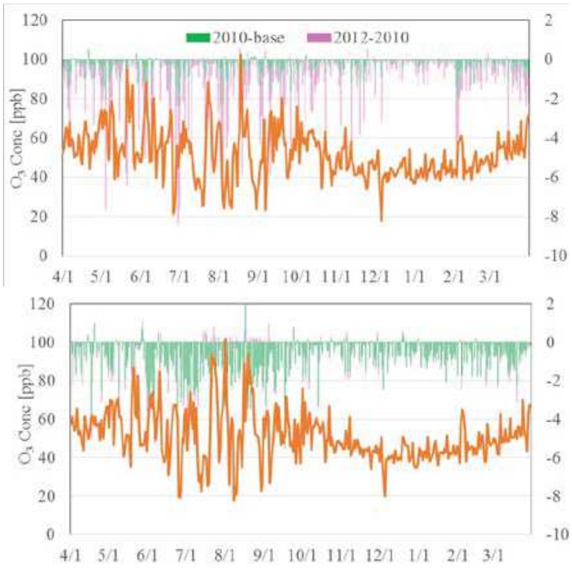

Fig.9 Time series of O_3 concentration and the contribution to O_3 from thermal power station at Kainan (top) and Kobe (bottom).

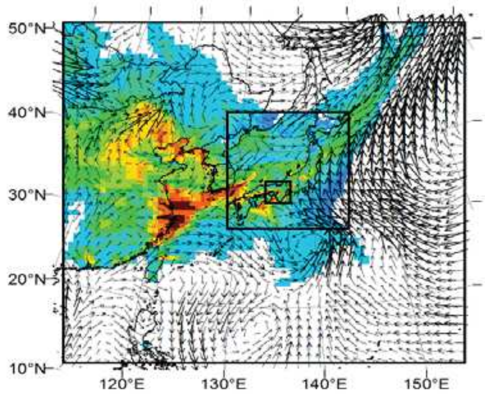

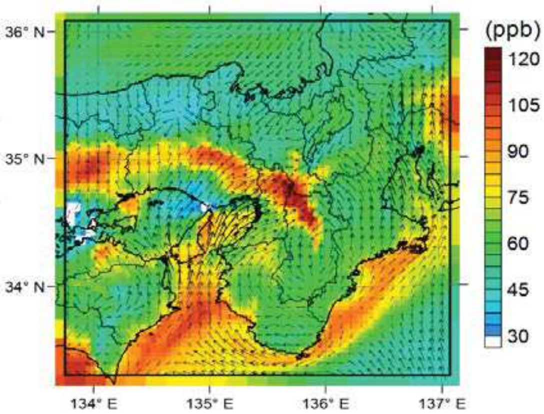

4. CONCLUSION

The simulations of air quality by the increased air pollutants from thermal power generation after

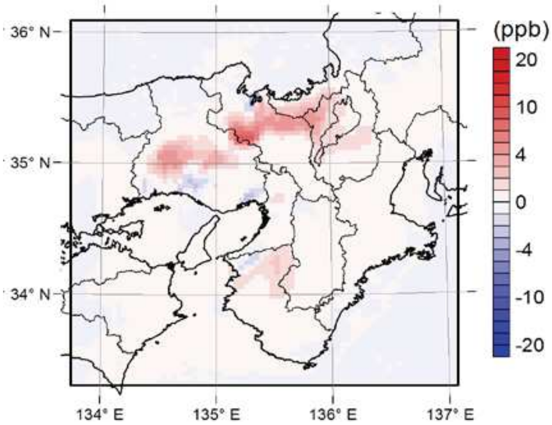

Fig.10 Distribution of O_3 concentration in D3 (Top) and D1 (Middle), and the distribution of the incremental O_3 concentration (Bottom) at 18 JST of 2 August

the Great East Japan Earthqu ake were carried out in the Kinki district by using WRF/CMAQ. The emissions of NOx and SO_2 from the thermal power stations after the Great East Japan Earthquake heavily increased. The simulations showed that (1) the remarkable increment of air pollution concentration of NO_2 and SO_2 was limited in the neighborhood of the thermal power stations, (2) the increment of O_3 concentration was widely spread but O_3 concentration in the neighborhood of the thermal power stations decreased because of NO titration.

4. REFERENCES

[1] URL:http://www.fepc.or.jp/library/pamphlet/zumenshu/
[2] URL:http://www.kepco.co.jp/sustainability/kankyou/report/data/karyoku01.html
[3] Fukui T., Kokuryo K., and et. al., Updating EAGrid2000-Japan emissions inventory based on the recent emission trends, Japan Society for Atmospheric Environment, 49, 2014, pp.117-125 (in Japanease).
[4] URL:http://www.kepco.co.jp/energy_supply/supply/denkiyoho/download.html.
[5] Emery C., Tai E. and Yarwood G.: Enhanced meteorological modeling and performance evaluation for two Texas ozone episodes. Prepared for The Texas Natural Resource Conservation Commission 12118 Park 35 Circle Austin, Texas 78753, 2001.